Evaluation of effective ground thermal conductivity for standing column well (SCW): Numerical modeling for in-situ TRT

Chulho Lee[1)], Jeehee Lim[2)], Myungsup Yoon[3)], Hangseok Choi*[4)]

[1), 2), 4)] *School of Civil, Environmental and Architectural Engineering, Korea University, Seoul, Korea*
[3)] *Energy Technology Center, Korea Testing Laboratory, Seoul, Korea*

[*] *hchoi2@korea.ac.kr*

ABSTRACT

The standing column well (SCW) is a viable option to utilize geothermal energy because it is thermally efficient and cost-effective. Evaluation of effective ground thermal conductivity is crucial in designing the SCW with consideration of subsurface hydraulics. This paper describes the full Navier-Stokes formulation to model the SCW numerically. Numerical modeling for the SCW has not been well developed due to its complexity of heat transfer and groundwater flow in the well and through ground formation. To simulate a coupled thermal and hydraulic (T-H) transfer surrounding the well, a two-dimensional axisymmetric numerical model was developed by assuming the ground formation as a porous medium. The numerical model was adopted in back-analyzing the effective ground thermal conductivity by numerically simulating in-situ thermal response tests (TRTs). The effect of hydraulic permeability of ground formation on the evaluation of the effective ground thermal conductivity from the TRT was extensively studied in this paper.

1. INTRODUCTION

The ground source heat pump (GSHP) system along with a ground heat exchanger (GHEX) is commonly used due to its straightforward mechanism. In winter, the ground temperature is higher than that of the atmosphere and heat energy is absorbed through the GSHP system. The collected heat is then used for space heating. In summer, the temperature in indoor spaces is higher than that of the ground and surplus heat energy is extracted and stored in the ground through the GHEX. The GSHP system can be divided into two categories: i.e., open-loop system and closed-loop system. The open-loop system uses surface water or groundwater in the subsurface as a heat carrier and circulates it through open ended pipes using pump. The closed-loop system adopts closed-loop pipes to circulate the fluid. Pipes are buried horizontally or vertically in the ground. Among open-loop systems, the standing column well (SCW) uses groundwater

---

[1)] Post-doctoral Researcher
[2)] Graduate Student
[3)] Research Engineer
[4)] Associate Professor

drawn from wells as a heat source or heat sink (Rees et al., 2004; Abu-Nada et al., 2008).

Conventional closed-loop GHEX's in geothermal applications are often modeled assuming no groundwater flow through the subsurface ground formation, that is soil/rock formations are considered as a solid (Rees et al., 2004). However, as shown in Fig. 1, the groundwater flow is benefical to the SCW system because it induces a heat transfer more effectively due to the additional advection in the ground formation. Fig. 1 shows heat transfer mechanisms in and around the SCW (Rees et al., 2004; Deng, 2004, Park et al., 2010). Because influence of groundwater flow to the overall heat transfer system is important in the SCW, interaction between the water in the borehole and groundwater should be precisely modeled. Unfortunately, current analytical or numerical solutions exclusively based on heat conduction cannot be directly applied to SCW simulations, in which groundwater flow has a significant influence on heat transfer, especially during bleeding operation.
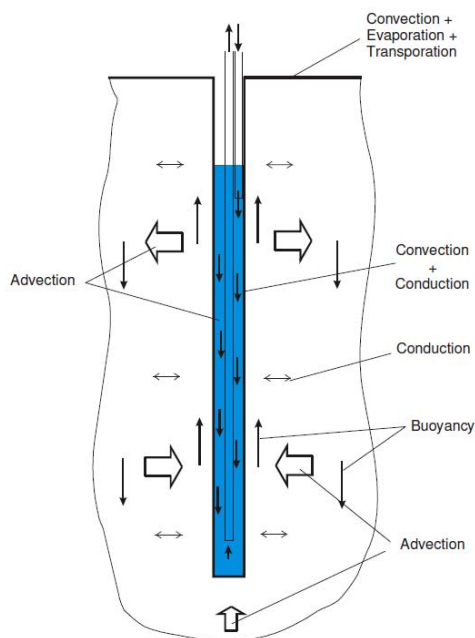
Fig. 1 Heat transfer mechanisms in SCW systems (Rees et al, 2001)

To evaluate ground thermal conductivity, an in-situ thermal response test (Gehilin, 2004) based on the infinite line source model (Carslaw and Jaeger, 1954) is typically performed as a simple means because to obtain entire thermal profile of the ground formation in the field is very expensive and time-consuming. However, the infinite line source model considers only pure heat conduction in the ground. Thus, the thermal conductivity estimated from TRT is often overestimated due to additional effect induced by the groundwater flow in the SCW system. Deng (2004) reported that the effective thermal conductivity of the ground evaluated from TRT is enhanced by the advection effect which depends on hydraulic conductivity and porosity of the ground formation, so called "enhanced thermal conductivity".

Numerical modeling for the SCW has not been well developed due to its complexity

of heat transfer and groundwater flow in the well and ground formation. In this study, to simulate a coupled thermal and hydraulic (T-H) transfer surrounding the well, two 2D axisymmetric numerical models are developed by assuming the ground formation as a porous medium. One uses the full Navier-Stokes formulation with the FORTRAN code and the other uses a conventional CFD (computational fluid dynamics) method. The developed numerical models are verified with previous researches. Then, the effective ground thermal conductivity was evaluated by numerically simulating in-situ thermal response tests (TRTs). The effect of hydraulic conductivity on the evaluation of the effective ground thermal conductivity from the TRT was extensively studied in this paper.

2. Non-Darcian Navier-Stokes Model

2.1. Modeling

The developed model considers an incompressible viscous fluid (density ρ_f, coefficient of viscosity μ_f, thermal conductivity k_f, specific heat at constant pressure C_p) circulating in the standing column well system. The ground formation outside of the bore hole is assumed as isotropic and homogeneous porous medium; with effective thermal diffusivity (k_{eff}), porosity (ε) and permeability (K). A cylindrical coordinate system (r^*, θ^*, z^*), with the velocity components (u^*, v^*, w^*), is adopted. In addition, a dimensional temperature variable (T) is considered in the model. The physical geometry and coordinate system are illustrated in Fig. 2. It is assumed that ground temperature is linearly distributed along with z^* and expressed as Eq. (1).
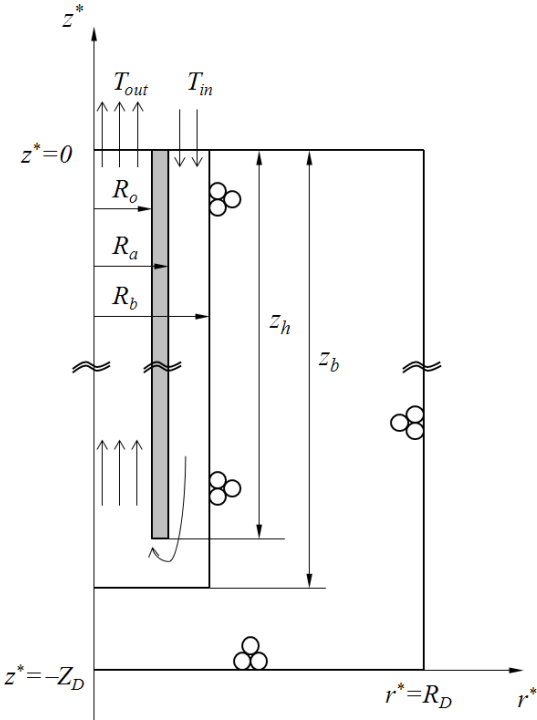
Fig. 2 Physical model configuration

$$T_w = T_o + C_1 z^*$$ (1)

Where T_o is the reference ground surface temperature and C_1 is the temperature gradient coefficient of ground. Then, the dimensional governing equations and boundary conditions are expressed as follows;

$$\frac{1}{r^*}\frac{\partial(r^* u^*)}{\partial r^*} + \frac{\partial w^*}{\partial z^*} = 0$$ (2)

$$\frac{\rho_f}{\varepsilon}\frac{\partial u^*}{\partial t^*} + \frac{\rho_f}{\varepsilon^2}\left(u^*\frac{\partial u^*}{\partial r^*} - \frac{v^{*2}}{r^*} + w^*\frac{\partial u^*}{\partial z^*}\right) = -\frac{\partial p^*}{\partial r^*} + \frac{\mu_{eff}}{\varepsilon}\left[\frac{1}{r^*}\frac{\partial}{\partial r^*}\left(r^*\frac{\partial u^*}{\partial r^*}\right) + \frac{\partial^2 u^*}{\partial z^{*2}} - \frac{u^*}{r^{*2}}\right]$$
$$-\left(\frac{\mu_f}{K} + \frac{\rho_f C}{\sqrt{K}}\sqrt{u^{*2}+v^{*2}+w^{*2}}\right)u^*$$ (3)

$$\frac{\rho_f}{\varepsilon}\frac{\partial v^*}{\partial t^*} + \frac{\rho_f}{\varepsilon^2}\left(u^*\frac{\partial v^*}{\partial r^*} + \frac{u^* v^*}{r^*} + w^*\frac{\partial v^*}{\partial z^*}\right) = \frac{\mu_{eff}}{\varepsilon}\left[\frac{1}{r^*}\frac{\partial}{\partial r^*}\left(r^*\frac{\partial v^*}{\partial r^*}\right) + \frac{\partial^2 v^*}{\partial z^{*2}} - \frac{v^*}{r^{*2}}\right]$$
$$-\left(\frac{\mu_f}{K} + \frac{\rho_f C}{\sqrt{K}}\sqrt{u^{*2}+v^{*2}+w^{*2}}\right)v^*$$ (4)

$$\frac{\rho_f}{\varepsilon}\frac{\partial w^*}{\partial t^*} + \frac{\rho_f}{\varepsilon^2}\left(u^*\frac{\partial w^*}{\partial r^*} + w^*\frac{\partial w^*}{\partial z^*}\right) = -\frac{\partial p^*}{\partial z^*} + \frac{\mu_{eff}}{\varepsilon}\left[\frac{1}{r^*}\frac{\partial}{\partial r^*}\left(r^*\frac{\partial w^*}{\partial r^*}\right) + \frac{\partial^2 w^*}{\partial z^{*2}}\right]$$
$$-\left(\frac{\mu_f}{K} + \frac{\rho_f C}{\sqrt{K}}\sqrt{u^{*2}+v^{*2}+w^{*2}}\right)w^* + \rho_f g\beta(T-T_w)$$ (5)

$$\frac{(\rho C_p)_{eff}}{(\rho C_p)_f}\frac{\partial T}{\partial t^*} + \left(u^*\frac{\partial T}{\partial r^*} + w^*\frac{\partial T}{\partial z^*}\right) = \frac{k_{eff}}{\rho_f C_f}\left[\frac{1}{r^*}\frac{\partial}{\partial r^*}\left(r^*\frac{\partial T}{\partial r^*}\right) + \frac{\partial^2 T}{\partial z^{*2}}\right]$$ (6)

Numerical solutions to the above partial differential equations were obtained by utilizing the well-established SIMPLER algorithm (Patankar 1980) with the QUICK scheme (Hayase et al. 1992) followed by discretization. Further numerical details can be referred to literature. At each time step, iteration continued until the relative changes of the flow rate and temperature between two consecutive iteration steps became less than 10^{-5}. In addition, the numerical calculation ceased when relative changes of each variable between two adjacent time steps were less than 10^{-4}. For convenience, non-dimensional factors are introduced as follows:

$$(u,v,w) = \frac{1}{U_o}(u^*,v^*,w^*), \quad (r,z) = \frac{1}{R_o}(r^*,z^*), \quad t = \frac{t^*}{t_o}$$

$$p = \frac{p^*}{\rho_f U_o^2}, \qquad \theta = \frac{(T_w - T)}{C_1 R_o}$$

In the above non-dimensional relations, R_o is the reference value for the radius of the pipe inlet, U_o is the reference value for the velocity in the cylindrical coordinate, and t_0 is the reference time. With these non-dimensional factors, the governing equations are shaped in simple forms as follows:

$$\frac{1}{r}\frac{\partial(ru)}{\partial r}+\frac{\partial w}{\partial z}=0 \tag{7}$$

$$\frac{R_o}{\varepsilon U_o t_o}\frac{\partial u}{\partial t}+\frac{1}{\varepsilon^2}\left(u\frac{\partial u}{\partial r}-\frac{v^2}{r}+w\frac{\partial u}{\partial z}\right)=-\frac{\partial p}{\partial r}+\frac{\mu_{eff}}{\varepsilon\mu_f}\frac{1}{Re}\left[\frac{1}{r}\frac{\partial}{\partial r}\left(r\frac{\partial u}{\partial r}\right)+\frac{\partial^2 u}{\partial z^2}-\frac{u}{r^2}\right]$$
$$-\left(\frac{1}{Re\,Da}+\frac{C}{\sqrt{Da}}\sqrt{u^2+v^2+w^2}\right)u \tag{8}$$

$$\frac{R_o}{\varepsilon U_o t_o}\frac{\partial v}{\partial t}+\frac{1}{\varepsilon^2}\left(u\frac{\partial v}{\partial r}+\frac{uv}{r}+w\frac{\partial v}{\partial z}\right)=\frac{\mu_{eff}}{\varepsilon\mu_f}\frac{1}{Re}\left[\frac{1}{r}\frac{\partial}{\partial r}\left(r\frac{\partial v}{\partial r}\right)+\frac{\partial^2 v}{\partial z^2}-\frac{v}{r^2}\right]$$
$$-\left(\frac{1}{Re\,Da}+\frac{C}{\sqrt{Da}}\sqrt{u^2+v^2+w^2}\right)v \tag{9}$$

$$\frac{R_o}{\varepsilon U_o t_o}\frac{\partial w}{\partial t}+\frac{1}{\varepsilon^2}\left(u\frac{\partial w}{\partial r}+w\frac{\partial w}{\partial z}\right)=-\frac{\partial p}{\partial z}+\frac{\mu_{eff}}{\varepsilon\mu_f}\frac{1}{Re}\left[\frac{1}{r}\frac{\partial}{\partial r}\left(r\frac{\partial w}{\partial r}\right)+\frac{\partial^2 w}{\partial z^2}\right]$$
$$-\left(\frac{1}{Re\,Da}+\frac{C}{\sqrt{Da}}\sqrt{u^2+v^2+w^2}\right)w-\frac{Ra}{Re}\theta \tag{10}$$

$$\sigma\frac{R_o}{U_o t_o}\frac{\partial\theta}{\partial t}+\left(u\frac{\partial\theta}{\partial r}+w\frac{\partial\theta}{\partial z}\right)-w=\frac{1}{RePr}\left[\frac{1}{r}\frac{\partial}{\partial r}\left(r\frac{\partial\theta}{\partial r}\right)+\frac{\partial^2\theta}{\partial z^2}\right] \tag{11}$$

Model geometric parameters are summarized in Table 1, and thermal and hydraulic material properties are rendered in Table 2.

Table 1 Dimensional and non-dimensional geometric parameters

	Dimensional value	Non-dimensional value
Depth of domain Z_D	350 m	6889.76
Radius of domain R_D	160 m	3149.61
Inner radius of pipe R_o	50.8 mm	1
Outer radius of pipe R_a	57.15 mm	1.125
Depth of pipe z_h	318 m	6259.84
Depth of borehole z_b	320 m	6299.21
Radius of borehole R_b	76.2 mm	1.5

Table 2 Relevant thermal and hydraulic properties

Thermal conductivity of pipe (k_{pipe})	3.81 W/mK
Heat capacity of pipe ($(\rho C_p)_{pipe}$)	4180 kJ/m^{3}K
Themal conductivity of fluid (k_f)	0.6 W/mK
Heat capacity of fluid ($(\rho C_p)_f$)	4180 kJ/m^{3}K
Kinematic viscosity of fluid (ν_f)	1.0×10^{-6} m^2/s
Thermal coductivity of solid ground (k_s)	3.81 W/mK
Ground temperature gradient(C_1)	0.0225
Heat capacity of solid ground ($(\rho C_p)_s$)	4180 kJ/m^{3}K
Porosity of ground (ε)	0.275
Mass flow rate (m')	0.160 kg/s
Effective thermal coductivity of ground (k_{eff})	2.927 W/mK

2.2. Model Verification

To validate the non-Darcian Navier-Stokes' formulations developed in this study, a series of comparisons was made with reference to the porous pipe flow study by Kumar et al (2011). From Fig. 3 through Fig. 4, the non-Darcian Navier-Stokes' calculations are performed without considering the subsurface ground formation, which means the calculation domain is exclusively within the borehole. In other words, no-penetration and temperature boundary conditions are applied on the borehole boundary (i.e., $r^*=R_b$, $z^*=-z_b$). Flow velocity inside of the borehole casing calculated from the non-Darcian Navier-Stokes' formulations is showed in Fig. 3 especially near the top and bottom of the casing. Discharge flow from the surface occurs downward (right-handed arrows in Fig. 3 (a1) & (b1)) and returns upward near the end of the casing (left-handed arrows in Fig. 3 (a2) & (b2)). The buoyancy-involved flow pattern appears near the inner pipe in a fully developed returning flow region (Fig. 3 (b1)), whereas there are no flow differences in the initial return flow regions (Fig. 3 (a2) & Fig. 3 (b2)). A series of comparisons with the analytical solutions provided by Kumar et al. (2011) is delineated in Fig. 4. There are no data comparisons in the range of $1.0 < r < 1.5$, since Kumar et al. (2011) solved simple one-way flows without returning in their analytical solutions. In the pipe wall region ($1.0 < r < 1.125$), no-penetration solid treatment and infinite thermal conductivity ($Pe_s \rightarrow 0$) with $\theta=0$ are numerically imposed. For the variable parameters of Rayleigh number (Ra), Forchheimer number (F') and Darcy number (Da), the current results shows a good agreement with the Kumar et al. (2011) works so that the numerical model is assumed to be feasible to simulate TRT's performed in SCW.
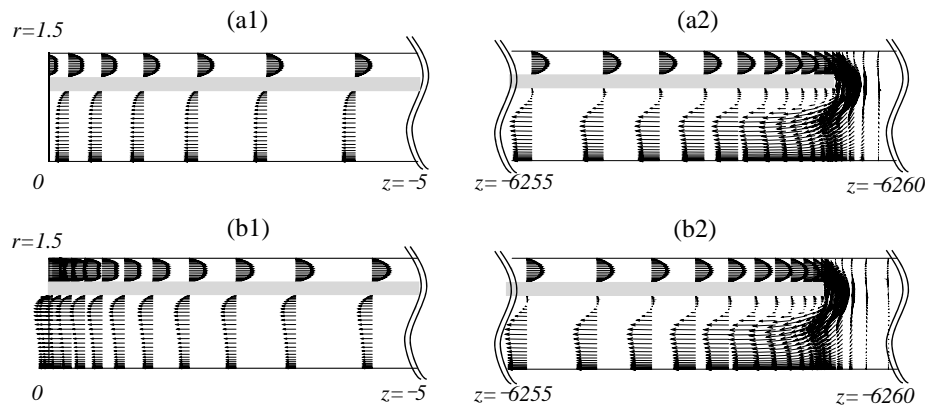
Fig. 3 Flow velocity near the top of borehole casing ((a1), (b1)) and near the bottom of the borehole casing ((a2), (b2)): (a) No buoyancy flow pattern (Ra=0), (b) Buoyancy-involved flow pattern
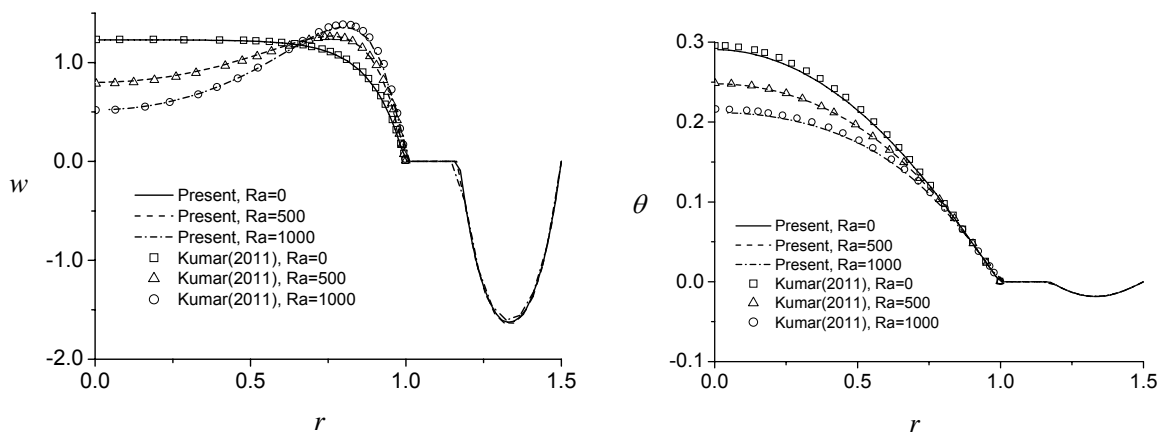
Fig. 4 Non-Darcian Navier-Stokes formulation validation with analytic solution of Kumar et al. (2011): Vertical velocity (w) and temperature profile (θ) at Da=10^{-2}, F'=10^{2}

3. Commercial CFD numerical model

3.1. Modeling

To simulate SCW, the conventional CFD program, FLUENT, was additionally adopted. The boundary conditions of SCW and ground formation are imported from Mikler (1993) of which experimental data is often used to verify numerical models developed in recent researches (Deng, 2004; Park et al., 2009). Fig. 5 shows a 2D axisymmetric model in CFD simulations and Table 3 summarizes borehole properties including the geometries well and pipes. The groundwater level is assumed to exist 30 m below from the ground surface, and the well length extends 320 m from the surface. In addition, the well diameter is modeled as 0.15 m.
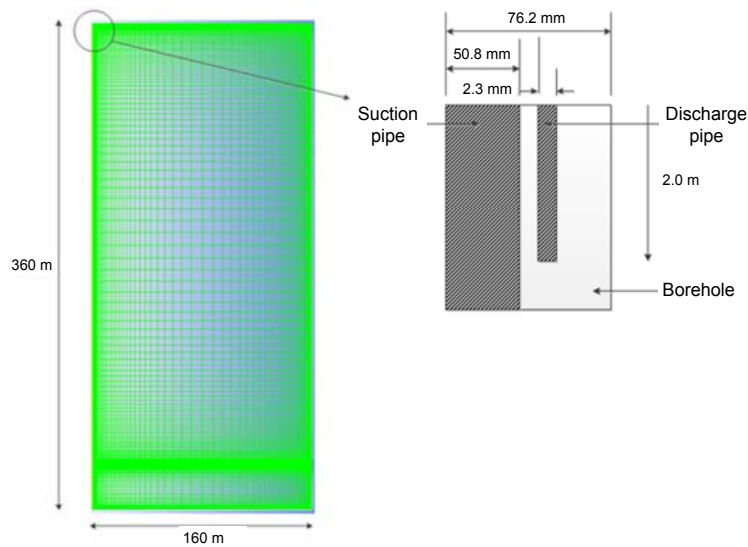
Fig. 5 2D axisymmetric model in CFD simulations

Table 3 Properties of the borehole

	Borehole	Discharge pipe	Suction pipe
Depth	320m	2m	318m
Diameter	152.4mm	33.4mm	101.6mm
Wall Thickness	—	3.05mm	6.35mm
Thermal Conductivity	—	4W/mK	0.1W/mK
Surface Roughness	1.5mm	1.5mm	1.5mm

For simplicity, it is commonly assumed that overall fluid flow in and around SCW as a laminar flow. However, the fluid flow in pipes and well should be treated as a turbulent flow due to wall friction effect and high velocity. Therefore, the current paper modifies the fluid flow in pipes and well by introducing effective hydraulic conductivity originated from Chen (1979) and Chen and Jiao (1999) as follows.

$$k_{eff} = \begin{pmatrix} k & \text{ground} \\ \dfrac{d^2 \rho_f g}{32 \mu} & \text{pipe} \\ \dfrac{2gd}{uf} & \text{well} \end{pmatrix} \qquad (12)$$

where, d = well diameter, ρ_f = fluid density, g = the acceleration of gravity, μ = viscosity, u = average flow velocity in well, f = the coefficient of wall friction.

The ground is modeled as a porous medium by including a porosity term to allow groundwater flow surrounding the SCW. The heat transfer equation in the ground is described as follows (FLUENT, 2012):

$$\frac{\partial}{\partial t}(n\rho_f E_f + (1-n)\rho_s E_s) + \nabla(\vec{v}(\rho_f E_f + p)) = \nabla\left[k_{eff}\nabla T - \left(\sum_i h_i J_i\right) + \left(\overline{\overline{\tau}}\vec{v}\right)\right] + S_f^h \quad (13)$$

where, k_{eff} = the effective thermal conductivity of porous medium, T = temperature, h = enthalpy, J = diffusion flux, n = the porosity of medium, E_f = energy in fluid, E_s = energy in solid, ρ_s = solid density, S_f^h = the enthalpy of fluid.

The effective thermal conductivity of the porous medium can be evaluated by applying a volume fraction average.

$$k_{eff} = \varepsilon k_f + (1-\varepsilon)k_s \quad (14)$$

where, k_f = the thermal conductivity of fluid, k_s = the thermal conductivity of solid.

Table 4 presents the thermal and hydraulic properties of the ground formation adopted for verifying the numerical model developed in this paper. To evaluate groundwater effect, two cases with different values of hydraulic conductivity are considered in this study; i.e., 7×10^{-5} m/s and 1×10^{-5} m/s.

Table 4 Hydraulic and thermal properties of the ground formation

Thermal Properties		Hydraulic Properties	
Thermal conductivity (k_s)	3.81 W/mK	Hydraulic conductivity	7×10^{-5} m/s and 1×10^{-5} m/s
Ground temperature	T(K) = 289.15+0.0225×depth(m)	Porosity	27.5%
Density	2700 kg/m3		
Specific Heat	1000 J/kgK		

To account for ground temperature variation with depth (i.e., geothermal gradient) and input boundary conditions for simulating fluid circulation with different temperatures, user-defined functions (UDF) were adopted in the CFD model. The increase in ground temperature with depth is applied from the top of the model (that is the ground surface)

to the bottom of the model using Eq. (15). In addition, the upper surface boundary of the ground is assumed as a no-flux boundary.

$$\text{Ground temperature [K]} = 289.15 \text{ [K]} + 0.0225 \text{ [K/m]} \times \text{depth [m]}. \qquad (15)$$

3.2. CFD *Model Verification*

To verify the CFD model developed in this paper, the field data provided by Mikler (1993) was used. The numerical simulations with the hydraulic conductivities of 7×10^{-5} m/s and 1×10^{-5} m/s were compared with the field monitoring results. Deng (2004) and Park et al. (2009) selected the hydraulic conductivity of 7×10^{-5} m/s to simulate the field monitoring from Mikler (1993). However, because the literature value of 7×10^{-5} m/s was not directly measured in the field test, two different hydraulic conductivities were considered in this study to verify the previous suggestion and tried to find more reasonable values. As shown in Fig. 6, the outlet temperature is varied with the hydraulic conductivity of the ground. It is observed that when the hydraulic conductivity of 1×10^{-5} m/s instead of 7×10^{-5} m/s is applied to the Mikler (1993) case, the numerical simulation is in better agreement with the field monitoring data.
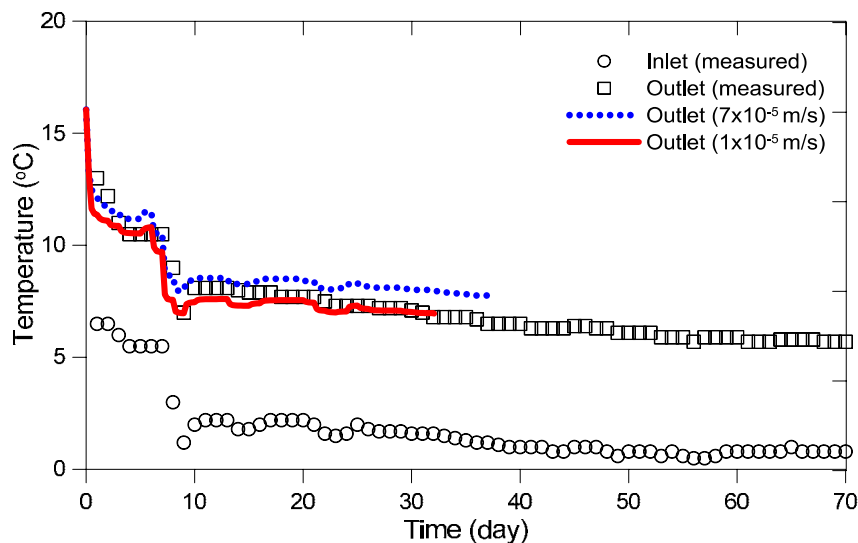
Fig. 6 The comparison between numerical simulation and field monitoring data (Mikler, 1993)

4. Inverse Parameter Estimation from TRT

A series of back-analyses for the effective thermal conductivity of the ground formation was performed by numerically simulating in-situ thermal response tests (TRTs) both with the Non-Darcian Navier-Stokes model and the CFD numerical model. After simulation for TRTs, the infinite line source model was adopted to evaluate the effective thermal conductivity of the ground formation. To manipulate the infinite line source model, the average temperature of circulating fluid as a function of time ($T_f(t)$) is to represent the temperature in the well circumference. Hence, the effective ground

thermal conductivity (λ) according to the line source model can be evaluated from the slope (m) of a straight line plotted in the T_f - $\ln(t)$ graph [Gehlin, 2002; Lee et al., 2011].

$$\lambda = \frac{q}{4\pi m} = \frac{q}{4\pi} \frac{\ln(t_2) - \ln(t_1)}{T_f(t_2) - T_f(t_1)}$$ (16)

To apply a constant rate of heat injection to the GHEX, the fluid temperature entering into the discharge pipe is evaluated using Eq. (17) as an inlet boundary condition variable with time. In this paper, 120 kW of heat injection rate was considered as an input power.

$$\text{Input Power [kW]} = C_p \times m' \times (T_{in} - T_{out})$$ (17)

where C_p= the specific heat of fluid, m' =mass flow rate, T_{in}= fluid temperature entering into discharge pipe, T_{out}= fluid temperature leaving from suction pipe.

The ground formation surrounding the SCW can be treated by solid or porous media. As for the Non-Darcian Navier-Stokes model, the ground formation is basically modeled as a solid medium by setting Darcy number (Da) to be infinite (i.e, $Da \rightarrow \infty$) to eliminate the Darcy and Forchheimer terms in the governing equation. The porosity of ground formation is set to be 1 for the solid treatment. The Prandtl number of the fluid ($\text{Pr}_f = v_f / \alpha_f$) inside the borehole and of the effective ground ($\text{Pr}_{eff} = v_f / \alpha_{eff}$) is selected as 6.967 and 1.428, respectively.

On the other hand, the ground formation can be modified to be a porous medium by considering the Darcy and Forchheimer terms together. For example, the porosity of ground formation is assumed 0.275, the effective thermal conductivity (k_{eff} = (1-ε)k_s+ε k_f = 0.725x3.81+0.275x0.6) is calculated as 2.927. In this case, a very small Darcy number is of interest ($Da \rightarrow 0$). This is an idealized case where the ground with porosity 0.275 is homogeneously saturated with water, but the porous ground formation has very small hydraulic conductivity. It is conceptually identical with the solid ground modeling. In other words, the solid ground model ($Da \rightarrow \infty$, ε =1, with effective ground properties) is comparable with the special case of the porous model($Da \rightarrow 0$, ε =0.275). Fig. 7 verifies the preceding modeling hypothesis. The TRT simulations for the two different models show a little discrepancy each other, and the logarithmic fitting slopes have a relative percent error of 3.5%. For the special case of porous model, λ is calculated as 2.432.
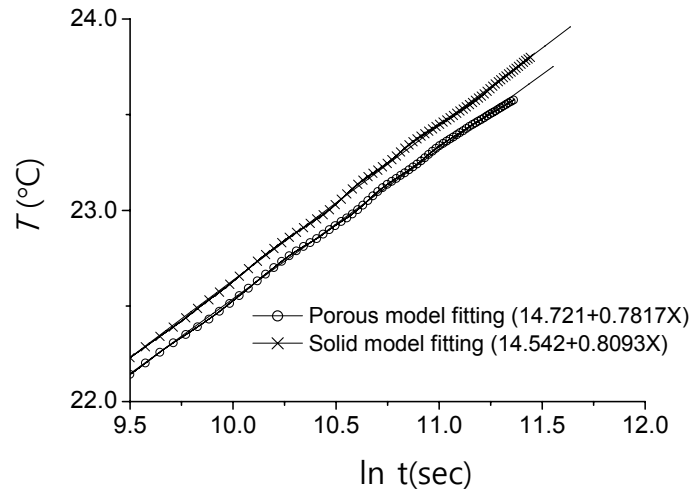
Fig. 7 Comparison of thermal response test (TRT) simulations between porous modeling and solid modeling

Fig. 8 shows thermal response curves for different hydraulic conductivities: i.e., 1×10^{-45} m/s, 1×10^{-5} m/s and 7×10^{-5} m/s). The cases represent the corresponding non-dimensional Darcy numbers with the length scale (R_o) of 3.95×10^{-50}, 3.95×10^{-10} and 2.77×10^{-9}, respectively, according to $K(\text{m}^2) = h_c \mu_f / (\rho_f g)$ and $Da = K/R_o^2$. For different hydraulic conductivities, λ is calculated from the logarithmic fitting slopes in Fig. 8 as follows: λ = 2.458, 3.254 and 7.583 for $h_c = 1 \times 10^{-45}$, 1×10^{-5} and 7×10^{-5}, respectively.
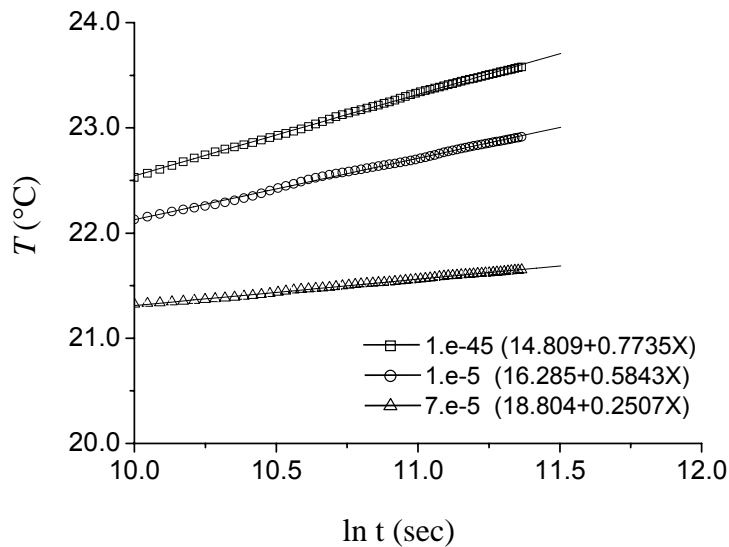
Fig. 8 Comparison of thermal response test (TRT) simulations for different hydraulic conductivities

As for the CFD numerical model, a back-analysis was carried out to verify the applicability of TRT for the SCW. The ground formation was treated as both solid and porous medium. The thermal conductivity of solid portion in the ground formation is arbitrary selected as 3.81 W/mK.

Fig. 9 shows a numerical simulation for TRT with assumption of the solid ground formation. The infinite line source model is applied to estimate the effective thermal conductivity of the ground formation which is calculated as 3.45 W/mK by ignoring early 8 hours during the test. The effective thermal conductivity is estimated about 10% smaller than the thermal conductivity of the solid portion in the ground formation (i.e., solid ground). The result agrees with the tendency which is observed in a typical GHEX. The intrinsic limitation of the line source model that simplifies a GHEX assemblage as an infinitely long line source in the homogeneous material is considered as a main reason for this small discrepancy (Lee et al., 2011).
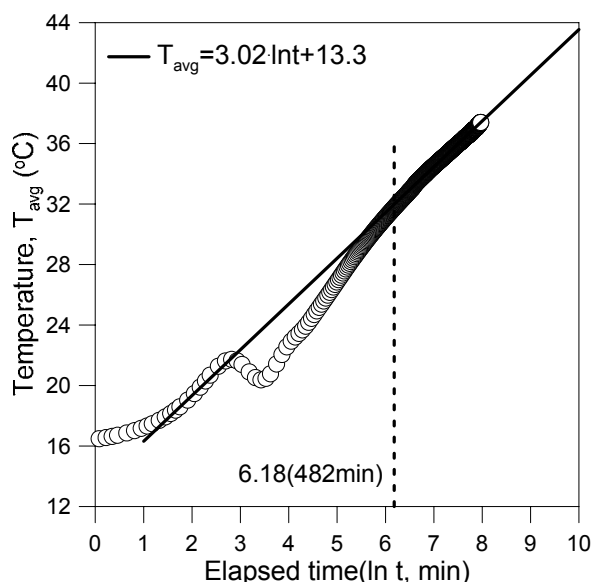
Fig. 9 Thermal response of TRT simulation for solid ground model

Fig. 10 illustrates two numerical simulations for TRT's with assumption of a porous ground formation along with different hydraulic conductivities. In modeling a porous medium, the thermal conductivity of the ground formation with the typical porosity of 0.275 is calculated as 2.93 W/mK according to Eq. (14) accompanied by the thermal conductivity of the solid (k_s) of 3.81 W/mK and the thermal conductivity of the fluid (k_f) of 0.62 W/mK. From the simulation results, the effective thermal conductivities are evaluated as 16.78 W/mK (about 470% greater than the thermal conductivity of the ground formation) and 3.23 W/mK (about 10% greater than the thermal conductivity of the ground formation) with the hydraulic conductivity of 7×10^{-5} m/s and 1×10^{-5} m/s, respectively. With the hydraulic conductivity of 7×10^{-5} m/s, the thermal conductivity of the ground formation is highly overestimated and even unrealistic compared to the typical thermal conductivity of rocks. However, as for the simulation result with the hydraulic conductivity of 1×10^{-5} m/s, it is considered to provide a reasonable trend when comparing with the results by Deng (2004).
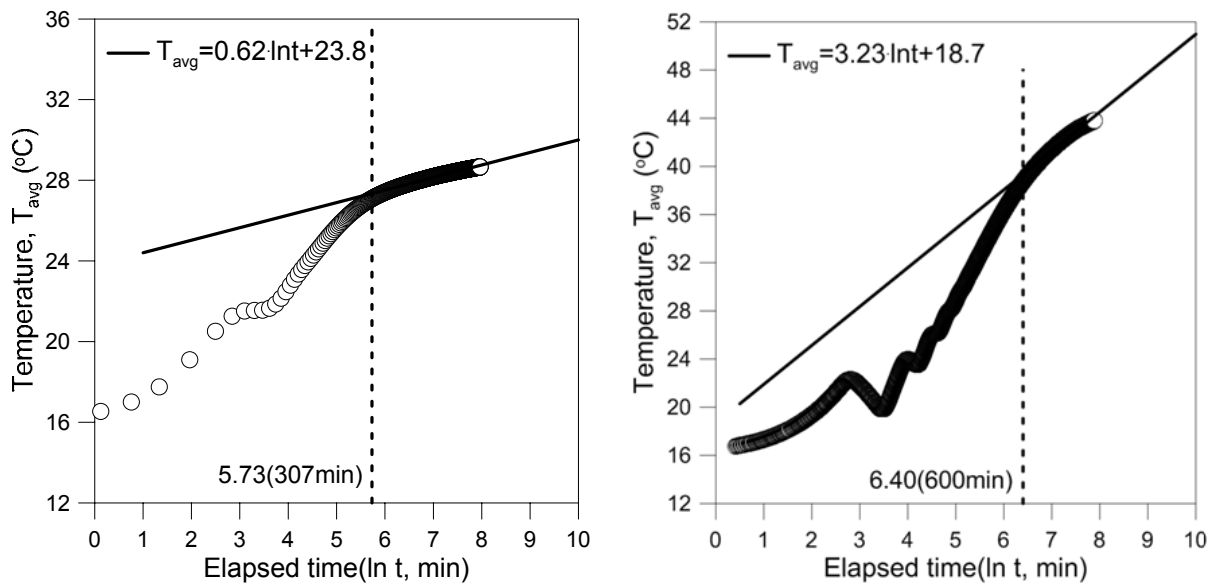
Fig. 10 Thermal response of TRT simulation for porous ground model

A summary of the inverse parameter estimation from TRT's by means of the Non-Darcian Navier-Stakes model and the CFD numerical model is presented in Table 5.

Table 5 Summary of the inverse parameter estimation

	k_s (W/mK)	ε (%)	k_{eff} (W/mK)	λ (W/mK)	Difference rate (%)
Solid Ground (hydraulic conductivity= 0 m/s)					
Non-Darcian Navier-Stokes model	3.81	27.5	2.93	2.43	-17
CFD numerical model	3.81	0	3.81	3.45	-9.4
Porous Ground (hydraulic conductivity= 1×10^{-5} m/s)					
Non-Darcian Navier-Stokes model	3.81	27.5	2.93	3.25	+11
CFD numerical model	3.81	27.5	2.93	3.23	+10
Porous Ground (hydraulic conductivity= 7×10^{-5} m/s)					
Non-Darcian Navier-Stokes model	3.81	27.5	2.93	7.58	+159
CFD numerical model	3.81	27.5	2.93	16.78	+473

In the solid ground model, the effective thermal conductivities back-analyzed from the TRT simulations are smaller than the thermal conductivity of the solid ground formation input in the model. On the contrary, in the porous ground model, the trend is vice versa.

Deng (2004) reported that enhancement of the effective thermal conductivity, so called "enhanced thermal conductivity", is usually observed in SCW and it depends on the hydraulic conductivity and porosity of the ground formation. The hydraulic conductivity of 1×10^{-5} m/s gives more reasonable results in comparison with the suggestions from Deng (2004).

In consequence, the hydraulic conductivity of a porous ground formation (that is a "real" ground formation) plays an important role in estimating the effective thermal conductivity from TRT results. Therefore, it is highly recommended that the effective thermal conductivity evaluated from in-situ TRT data be properly modified to be used as an input value for SCW designs.

CONCLUSION

Two different models for evaluating the effective thermal conductivity of the ground formation are developed in order to design the SCW. The models enable back-analyze the effective thermal conductivity of the ground formation from TRT results. The obtained results are summarized as follows:

Conventional closed-loop GHEX's are satisfactorily modeled by assuming no groundwater flow through the subsurface ground formation. However, groundwater flow is beneficial to the SCW system because it induces an additional heat transfer by advection in the ground formation. Because influence of groundwater flow to the overall heat transfer system is important in the SCW, interaction between the water in the borehole and groundwater should be precisely modeled.

The effective thermal conductivities back-analyzed from the TRT simulations are smaller than the thermal conductivity of the solid ground formation when the ground formation is modeled as a solid medium. However, in the porous ground model, the back-analyzed effective thermal conductivity is greater than the porous ground formation due to the enhanced thermal conductivity.

It can be concluded that the hydraulic conductivity of the ground formation has considerable effect on the estimation of the effective thermal conductivity of the porous ground. Especially, as for the CFD numerical simulation, the numerical analysis is very sensitive to the hydraulic conductivity.

ACKNOWLEDGMENTS

REFERENCES

Chen, C., and Jiao, J.J. (1999), "Numerical simulation of pumping tests in multiplayer

wells with non-darcian flow in the well bore", Groundwater, Vol.37, No.3, pp.465-474.

Deng, Z. (2004), *Modeling of standing column wells in ground source heat pump systems*, Ph.D. Thesis, Oklahoma State University.

FLUENT (2012), ANSYS manual Ver. 13.0, ANSYS, Inc. Products

Gehlin, S., (2002), Thermal response test—method development and evaluation, Doctoral Thesis 2002:39. Lulea University of Technology, Sweden

Hayase, T., J. A. C. Humphrey & R. Grief (1992), *A consistently formulated QUICK scheme for fast and stable convergence using finite-volume iterative calculation procedures*, J. Comput. Phys., 1992; 98: 108-118.

Kumar, A., P. Bera, J. Kuma (2011), "Non-Darcy mixed convection in a vertical pipe filled with porous medium", *Int. J. Thermal Sciences*, 2011; 50: 725-735.

Lee, C., Park, M., Min, S., Kang, S-H, Sohn, B., Choi, H. (2011) "Comparison of Effective Thermal Conductivity in Closed-Loop Vertical Ground Heat Exchangers" Applied Thermal Engineering 31(17-18), 3669-3676

Mikler, V. (1993), *A theoretical and experimental study of the "energy well" performance*, Master thesis, The Pennsylvania State University.

Orio, C. (1995), "Design, use and examples of standing column wells", *IGSPHA Technical Meeting*

Park, D-H, Kim, K-K, Kwak, D-Y, Chang, J-H and Park, S-S (2010), "Numerical Simulation of Standing Column Well Ground Heat Pump System Part 1: Validation of the Numerical Model", *J. of KSGE* **26**(2), 33~43, in Korean.

Patankar, S. V. (1980), *Numerical heat transfer and fluid flow*, Hemisphere/McGrawHill, New York

Rees, S. (2001), "Advances in modeling of standing column wells", *International Ground Source Heat Pump Association Technical Conference & Expo*, Stillwater, Oklahoma

Rees, S.J., J.D. Spitler, Z. Deng, C.D. Orio and C.N. Johnson (2004), "A Study Of Geothermal Heat Pump And Standing Column Well Performance", ASHRAE Transactions, 110(1), 3~13